Available online at www.sciencedirect.com
ScienceDirect
Catalysis Today 136 (2008) 93–103
CATALYSIS TODAY
www.elsevier.com/locate/cattod

Modeling of NO oxidation and NO_x storage on $Pt/BaO/Al_2O_3$ NO_x traps

Brian R. Kromer [a], Lei Cao [a], Lasitha Cumaranatunge [a], Shadab S. Mulla [a], Joshua L. Ratts [a], Alex Yezerets [b], Neal W. Currier [b], Fabio H. Ribeiro [a], W. Nicholas Delgass [a,*], James M. Caruthers [a,*]

[a] *School of Chemical Engineering, Purdue University, 480 Stadium Mall Drive, West Lafayette, IN 47907-2100, United States*
[b] *Cummins, Inc., 1900 McKinley Ave, Columbus, IN 47201, United States*

Available online 1 April 2008

Abstract

A one-dimensional model of NO oxidation and NO_x storage on $Pt/BaO/Al_2O_3$ monolith catalysts has been developed to predict evolution of the effluent gases as well as surface species during the storage portion of the NO_x trap cycle. The model combines separate descriptions of oxidation and storage. The oxidation portion of the model is based on a kinetic mechanism and quantitative parameters developed in our laboratory for a Pt/Al_2O_3 catalyst. Two NO_x storage models are proposed to account for the multiple time constants that control NO_x storage. A two site in series model was developed to account for diffusion into the bulk of Ba particles, while a two site parallel model was proposed to account for Ba sites close to Pt and those far from Pt. It is shown that both models adequately account for the asymmetric nature of the NO_x breakthrough curves and that current data cannot distinguish between the two models. It is also illustrated that external mass transfer plays a controlling role during early storage times and must be included in any model for the operating conditions used here. When possible, the model parameters were determined via independent experiments, while the remaining parameters were fit to the NO_x uptake data using a nonlinear least squares method.
© 2008 Published by Elsevier B.V.

Keywords: Kinetic modeling; NO_x storage; NO_x trap; NO oxidation

1. Introduction

Due to the ever increasing emissions standards for combustion engines continually better exhaust after-treatment technologies have been developed. An area of particular interest is that of lean burn engines. Lean burn gasoline or diesel engines are more fuel efficient than standard stoichiometric gasoline engines. However, because of the excess oxygen, conventional three-way catalysts cannot reduce NO_x compounds in the exhaust stream. One potential solution is the use of NO_x storage and reduction (NSR) catalysts [1–3]. These catalysts consist of a noble metal for oxidation and reduction of NO_x (e.g. Pt), and an alkaline or alkaline earth metal for storage of NO_x (e.g. Ba). The NSR catalyst is used with a cyclic engine operation, switching between long lean and short rich periods. During the lean period the catalyst oxidizes NO to NO_2 on the noble metal sites and stores the NO_x (NO and NO_2) on the alkaline earth sites. During the rich period, the NO_x is released from the storage sites and reduced to N_2 by the noble metal sites.

Because of the complex, dynamic nature of the NSR system it is highly desirable to have a model of the overall process that could make predictions both during the development of an improved after-treatment system and in an actual engine computer to control operation of the catalyst on stream. During the development stage a good interplay between experiments and modeling is necessary for efficient development of the improved after-treatment system. The model can be used to investigate the behavior of the catalyst under varying operating conditions, make predictions of the performance at these conditions, and to design new experiments for model validation. In addition, a model can provide insight into experimentally difficult to measure phenomena such as surface coverage or catalyst surface temperature. Once the final product is being used on the vehicle, the model could also be used in conjunction with the engine control module to facilitate the most efficient use of the engine and after-treatment system.

* Corresponding authors.
E-mail addresses: delgass@purdue.edu (W.N. Delgass), caruther@purdue.edu (J.M. Caruthers).

0920-5861/$ – see front matter © 2008 Published by Elsevier B.V.
doi:10.1016/j.cattod.2008.02.013

Several different models for the NSR system have been proposed in the literature. Olsson et al. [4–6] have proposed a mean field model of NO_x storage and a global kinetic model for both NO_x storage and catalyst regeneration. The proposed mean field model consists of a reaction network with a large number of reaction rate parameters. The problem was broken into five separate steps in order to simplify the modeling process. The model was fit to experimental data taken from flow reactor experiments, and a least squares fitting procedure was used to obtain the best fit. Their global kinetic model used reaction rates derived from mechanisms proposed in the literature. Diffusion in the washcoat was handled through the use of a shrinking core model on the barium particles. Both these models were solved using the tank in series method and solving the resulting algebraic CSTR equations.

Tuttlies et al. [7] developed a single particle model to study in detail the effects of diffusion and the formation of dense nitrate layers in the barium phase of the catalyst. From this analysis, a reactor channel model was proposed which includes both storage and regeneration. This was accomplished by using the concentration profiles obtained for single particles to model a bed of particles. This model was again solved using a tank in series approach and the parameters were fit to data obtained in an isothermal flat bed reactor which houses a thin slice of catalyst between heating plates. However, this analysis does not capture many of the effects of exothermicity on regeneration. For example, it has been proposed in the literature that the temperature rise could play a very important role in the release of NO_x species from the barium particles [2].

Other groups have also contributed to the NSR modeling literature. Koci et al. [8,9] and Crocoll et al. [10] have both developed 1D monolith models with complex mechanisms, ranging from 15 to 18 different reaction steps and at least that many rate parameters in an attempt to obtain an accurate description of the overall chemistry of the NSR system. Also, Daw et al. [11] proposed a storage model based on Freundlich isotherms, which were third order polynomial fits of adsorption data. The purpose of this model was to incorporate phenomena that can be measured experimentally with relatively simple experiments, while at the same time to be able to make predictions about storage in an actual lean NO_x trap. Also, Laurent et al. [12] and Sharma et al. [13] have made significant contributions to the modeling literature.

The present paper analyzes NO oxidation and NO_x storage in NSR catalysts using a one-dimensional model of a monolith reactor and is compared to in house experimental results obtained from model $Pt/BaO/Al_2O_3$ monolith catalysts. The model includes both gas phase and adsorbed species and accounts for surface reactions and boundary layer mass transport. A two layer approximation is utilized in order to account for diffusion effects within the washcoat. This assumption is shown to capture the experimental data quite well. The focus of the model development is to keep the model as simple as possible while capturing the important chemistry and physical phenomena of the real system. For the purpose of developing the model using a building up approach, we have chosen to omit any complications associated with the product molecules CO_2 and H_2O. These important effects are being studied and will be reported in a future paper.

2. Experimental methods

2.1. Reactor studies

Both NO oxidation and NO_x storage were studied. The detailed experimental setup for the oxidation studies is described elsewhere [14,15]. Oxidation experiments for this work were performed on the same setup used for the NO_x storage experiments, but with a Pt/Al_2O_3 catalyst. The catalyst used for NO_x storage was a $Pt/BaO/Al_2O_3$ (46 g/ft^3, 20%) washcoat deposited on a cordierite monolith consisting of 200 channels per square inch. The washcoat loading was 2.22 g/in.^{3} of the monolith. If the distribution of Pt and Ba is assumed to be uniform throughout the monolith, the weight loadings are 1.2% Pt, and 17.9% Ba within the washcoat. The experimental setup consists of a vertical bench-top, plug-flow stainless steel reactor. High-temperature Zetex insulation was wrapped around the catalyst (monolith) sample, and the assembly was placed in the reactor tube. The insulation material blocks the space between the monolith and the wall of the reactor, minimizing the gas flow bypassing the catalyst. Glass beads were placed upstream of the catalyst sample to ensure mixing and uniformity of the gas flow and the reactor was placed inside a clam shell temperature-controlled furnace. To minimize temperature gradients, the inlet gas was preheated before entering the reactor. Thermocouples were placed 6 mm before and after the catalyst sample to verify inlet and outlet gas temperatures. A reactor bypass loop after the pre-heater, and thus at the reactor conditions, was used for measurement of the inlet concentrations of the feed gases. All the gas lines were heated to 120–150 °C. Exit gases were analyzed using an FT-IR gas analyzer (Thermo Electron Corporation, Nicolet Antaris IGS). The FT-IR was set to measure a data point every second at a resolution of 0.5 cm^{-1}. The FT-IR is capable of monitoring NO, NO_2, N_2O, CO, CO_2, and H_2O gas concentrations, and the data was analyzed using the Nicolet TQ analysis software. The system is automated to control gas flows through mass flow controllers, switch valves between lean/rich cycles, and monitor the temperature output from the thermocouples using National Instruments LabVIEW software and FieldPoint units.

Preliminary work on the $Pt/BaO/Al_2O_3$-NSR catalyst consisted of long lean/rich cycles up to the point of saturation of the catalyst. That is, the lean period extended to the point where the NO_x slip through the catalyst is equivalent to the feed concentration. Here we chose to first understand the storage of NO_2 in the presence of O_2, N_2, and NO only. Commonly found exhaust gases such as CO_2 and H_2O which have been shown to compete for sites, and hence have a significant effect on storage [16], have not been considered in these initial experiments. The inlet O_2 concentration was held constant at 10% while the inlet NO_2 concentration was varied between 90 ppm and 390 ppm (balance N_2) and the temperature was held constant at 300 °C. The regeneration was done using 0.5% H_2 in N_2 for 300 s. This time period was sufficient to regenerate the catalyst completely

after long storage times (around 3000 s). The capture period varied, depending on the time to reach saturation which was governed by the inlet NO_x concentration. The total flow was maintained at 2.5 L min^{-1} (standard conditions) on a 1-in. long, 0.75 in. diameter monolith catalyst, yielding a space velocity of 20,700 h^{-1}.

2.2. DRIFTS studies

The catalyst used in the DRIFTS study was a Pt/BaO/Al_2O_3 (46 g/ft^3, 20%) washcoat deposited on a cordierite monolith consisting of 400 channels per square inch. The washcoat loading was 1.25 g/$in.^3$ of the monolith and assuming the components to be evenly distributed throughout the entire monolith, the weight loadings are 2.13% Pt, and 20% Ba within the washcoat. A piece was cut from the center of the monolith and filed down to a 4.5 mm wide circle with the top layer's walls removed so it could be placed in the sample cup. The sample was one channel deep with the infrared radiation focused on the top of the sample, i.e. the bottom of the exposed channel. A K-type thermocouple was placed in direct contact with the top of the sample to measure the temperature. Once the catalyst was loaded, it was heated to 500 °C in N_2 and held for 20 min. Then, the temperature was reduced to 400 °C and the catalyst was exposed to pure H_2 for 30 min. This procedure was used to decompose carbonates on the catalyst. Once the H_2 was shut off, the temperature was cooled to the desired temperature and the experiments were completed.

The experimental setup for the DRIFTS study is described elsewhere [17]. The gas flows of N_2, O_2, NO, and NO_2 were controlled by Porter Model 201 mass flow controllers and the gas flow of H_2 was controlled by a Brooks 5850 series mass flow controller. The flow of each gas from a manifold system to the DRIFTS cell was controlled by miniature solenoid three-way valves. The solenoid valves were controlled by a LabVIEW FieldPoint module and LabVIEW program to complete the lean/rich cycling. The diffuse reflectance (DR) spectra presented are the result of a series of multiple lean/rich cycles after they had become reproducible. The cycles used in this study were 15 min of capture, 4 min of an inert purge, 5 min of regeneration (1% H_2), and 4 min of an inert purge at a constant flow rate of 50 sccm. The inert purge was used to clear the dead volume in the DRIFTS cell to avoid mixing of the lean and rich front. The DR spectra are presented in Kubelka–Munk units with the experimentally collected reflectance defined elsewhere [17] and are the result of 32 scans averaged at a resolution of 4 cm^{-1}. The time spacing for the DR spectra was 12.78 s under these conditions.

The monolith used in the DRIFTS study was not the same monolith that was used for the modeling. The samples used in the DRIFTS experiments were cut from a different brick. However, the platinum and barium loadings were similar on a washcoat basis so it was assumed that the results from the DRIFTS study could be extended to the development of the model.

3. Modeling

Models for both NO_x uptake and NO oxidation were developed. A coupled model combining both phenomena has also been proposed. For all the models, the reactor is considered to be a single cylindrical monolith channel bounded by a washcoat layer and a cordierite wall. The channel has a radius of R_p. The radius including the channel and washcoat is R_w, and the whole tube including channel, washcoat and cordierite has radius R_0. Adsorption and reaction both occur only within the catalyst washcoat. A schematic of the tubular reactor is shown in Fig. 1.

3.1. Model assumptions and justifications

A number of significant assumptions are employed in order to simplify the model, yet maintain the important mathematical structure of the problem. They are described as follows:

(1) *Plug flow*: The radial dependence of the gas composition and gas temperature has been neglected. This assumption can be rationalized due to the large aspect ratio of the channel (L/R_p). The thermal and concentration boundary layers are implicitly incorporated through the use of heat and mass transfer correlations. However, the radial gradients are not explicitly incorporated into the model.
(2) *Constant gas velocity and no pressure drop along the reactor*: Because of the low concentrations of all of the NO_x species in the gas phase, the change of gas volume caused by absorption and reaction is negligible; therefore its effect on gas velocity is negligible. The effect of gas phase temperature change on the gas velocity is also neglected during the initial modeling efforts due to the isothermal assumption discussed later. Based on the laminar flow assumption and a flow velocity of 2 m s^{-1}, the pressure drop along the tube (2.5 cm) was estimated to be 10^{-4} atm. Therefore the pressure drop is also neglected.
(3) *Neglect axial dispersion in the gas phase*: The major contribution to mass transfer in the gas phase of the monolith is axial convection. That is especially true due to the large gas velocities used in these studies (~1 m/s). Because of this, axial dispersion is neglected for this model.
(4) *Neglect the diffusion barrier in the washcoat*: Only mass transfer through the boundary layer at the gas/washcoat interface is considered through the use of standard mass transfer correlations. This assumes that the gas phase

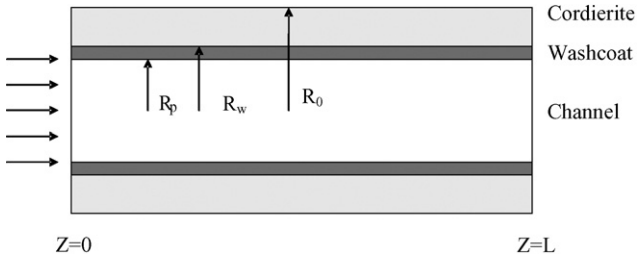

Fig. 1. A schematic of the monolith reactor used in the model.

concentration within the washcoat is constant in the radial direction which is reasonable because the washcoat layer is a relatively small volume when compared to the volume of the monolith channel. This assumption allows the model to be one-dimensional. It is well known, however, that diffusion into the bulk barium can play a significant role in the adsorption of NO_x species [18,19]. The diffusion into the bulk Ba is included in the model through the use of a two layer structure as discussed later, but, there is no explicit radial dependence in the model.

(5) *The monolith reactor is isothermal*: The monolith is assumed to be at a constant temperature throughout the NO_x storage phase. This assumption is used in order to mimic the isothermal conditions used for the experimental studies. Our experimental studies show that the gas phase temperature stays essentially constant during the trapping phase. This is also consistent with the high gas flow rates and low concentrations of reacting species.

These assumptions, along with a radially symmetric monolith channel, keep the equations of the model one-dimensional. However, due to the transient nature of the real process, the differential equations describing the process are time dependent.

3.2. General balance equations

3.2.1. Gas phase

The gas phase species balances include accumulation, convection and mass transport through the boundary layer. No reaction occurs in the gas phase mass balance. It is known that NO will react in the gas phase to form NO_2, however, according to a rate expression given by Tsukahara et al. [20], the gas phase reaction rate under the conditions used in our experiments is on the order of 10^{-16} mol L^{-1} s^{-1}. A comparison of this rate with a turnover rate on the catalyst of about 10^{-3} s^{-1} shows that the catalytic oxidation produces orders of magnitude more NO_2 than the gas phase reaction. This validates the assumption of no gas phase reaction. With these assumptions, the gas phase mass balance becomes:

$$\frac{\partial C_{gi}}{\partial t} = \frac{2k_m}{R_p}(C_{wi} - C_{gi}) - u\frac{\partial C_{gi}}{\partial z} \tag{1}$$

Here, C_{gi} is the gas phase concentration of species i, C_{wi} is the concentration in the washcoat (i.e. the species have crossed the boundary layer, but not yet adsorbed), k_m is the mass transfer coefficient and is obtained through experimental correlations [21], and u is the gas phase velocity. The corresponding initial and boundary conditions are

$$\begin{aligned} z = 0;\ C_{gi}(t) &= C_{gi}^{in} \\ t = 0;\ C_{gi}(z) &= C_{gi}^{ini} \end{aligned} \tag{2}$$

where C_{gi}^{ini} is the initial concentration (usually 0) and C_{gi}^{in} is the inlet concentration.

3.2.2. Washcoat

The mass balance in the washcoat accounts for accumulation, mass transfer from the gas phase, and adsorption to the catalyst surface. Since the gas phase in the washcoat layer can only fill the void space, the balance equation must also include the catalyst porosity. To keep the model one-dimensional, the volume of the washcoat is collapsed to a surface layer at the radius of the pore. In this case, the porosity of the washcoat is calculated in units of m^3 void space per m^2 of channel wall area. The washcoat species balance is written as

$$\frac{\partial C_{wi}}{\partial t} = \frac{k_m}{\varepsilon}(C_{gi} - C_{wi}) - \frac{1}{\varepsilon}r_i \tag{3}$$

where ε is the catalyst porosity in the washcoat, and r_i is the reaction rate of species i in units of mole m^{-2} s^{-1}. The initial and boundary conditions for the washcoat are

$$t = 0;\ C_{wi} = C_{wi}^{ini} \tag{4}$$

3.2.3. Surface

The one-dimensional nature of the model assumes that the three-dimensional porous catalyst network can be approximated by a two-dimensional surface which is then further reduced to one dimension through the assumption of axial symmetry. The total numbers of sites in the washcoat are assumed to be evenly distributed on a surface located at the channel radius. The concentration of surface species, C_i changes due to the reaction r_i, where the balance is given by

$$\frac{\partial C_{si}}{\partial t} = \bar{r}_i \tag{5}$$

where C_{si} is the surface concentration of species i on the catalyst washcoat, and $\bar{r}_i$ is the surface reaction rate. The initial conditions of surface species are

$$t = 0;\ C_{si} = C_{si}^{ini} \tag{6}$$

3.3. Solution method

The differential equations were solved using the FEMLAB Multiphysics Modeling software [22], now called COMSOL multiphysics. The FEMLAB software implements the finite element method for the solution of partial differential equations. Parameter optimization was performed using a nonlinear least squares parameter fitting toolbox within the MATLAB software [23].

4. Results and discussion

The following are the results of the actual numerical simulations as compared to the experimental data, as well as a discussion of the chemistry used to develop the various models. This comparison allows for the discrimination of the different mechanisms proposed for oxidation and storage. All unknown parameters were fit using the nonlinear least squares method discussed previously. Table 1 gives a summary of the values of

Table 1
Known constants used in the models

R_p	Channel radius	0.00071 m
R_w	Radius including washcoat	0.00075 m
L	Channel length	0.0254 m
T	Temperature	573 K
D	Gas phase diffusion coefficient	0.9 $cm^2\ s^{-1}$
L_{Pt}	Platinum site density	0.062 mol m^{-2}
k_{m2}	Second surface mass transfer coefficient	0.012 s^{-1}
$\tilde{k}_3$	Oxidation rate constant for (11)	0.00236 s^{-1}
K	Equilibrium constant for (11)	25.77
k	Oxidation rate constant for (12)	$9.15 \times 10^{-5}\ s^{-1}$
ε	Washcoat porosity	4.1×10^{-5} m

Table 2
Parameters for NO_x storage models

Series model		
k_f	Adsorption rate constant	$18.89 \pm 3.59\ m^3\ mol^{-1}\ s^{-1}$
L_{Total}	Total barium site density	0.0406 ± 0.0023 mol m^{-2}
L_2/L_1	Ratio of 2nd to 1st layer site density	4.08 ± 0.42
Parallel model		
k_{f1}	Rate constant for fast adsorption sites	$10.39 \pm 2.85\ m^3\ mol^{-1}\ s^{-1}$
k_{f2}	Rate constant for slow adsorption sites	$0.563 \pm 0.028\ m^3\ mol^{-1}\ s^{-1}$
L_{Total}	Total barium site density (fixed)	0.0406 mol m^{-2}
L_2/L_1	Ratio of slow sites to fast sites	2.58 ± 0.14

the model constants that were set by the experiment or determined by independent experiments. Table 2 is a list of the fitted parameters, with 95% confidence intervals, for the storage models to be discussed below. All parameters for the NO oxidation model are taken directly from [14,15].

4.1. NO oxidation

Since the adsorption of NO_2 is more favorable on the NSR catalyst than is the adsorption of NO [2], the oxidation of NO becomes an important step in the overall performance of the NO_x reduction system. We have chosen to examine NO oxidation as a starting point for the model. This is because the oxidation of NO can be studied independently of NO_x adsorption by removing the alkaline or alkaline earth component of the catalyst. Several different mechanisms for NO oxidation have been proposed in the literature; including both Langmuir–Hinshelwood and Eley–Rideal type mechanisms [6,10,24,25]. However, due to the previous work done in our laboratory on NO oxidation, we used steady state reaction expressions derived from our previous kinetic studies [15], which eliminates determination of the kinetic parameters for oxidation.

The steady state rate expressions can be derived from the following mechanism proposed by Mulla et al. [15]:

$$NO + * \overset{K_1}{\rightleftharpoons} NO* \tag{7}$$

$$NO_2 + 2* \overset{K_2}{\rightleftharpoons} NO* + O* \tag{8}$$

$$O_2 + * \underset{k_{-3}}{\overset{k_3}{\rightleftharpoons}} O_2* \tag{9}$$

$$O_2** + * \underset{k_{-4}}{\overset{k_4}{\rightleftharpoons}} 2O* \tag{10}$$

Here, (7), (8), and (10) are assumed to be in quasi-equilibrium, while (9) is assumed to be the rate determining step (RDS). Also, O* is taken as the most abundant surface intermediate. With these assumptions, the following expression is obtained for the forward rate:

$$r = \tilde{k}_3 \frac{C_{gO_2}}{1 + K(C_{gNO_2}/C_{gNO})} \tag{11}$$

where $K = K_2/K_1$ and $\tilde{k}_3 = k_3 L_s$. Assuming a high oxygen coverage on the surface, i.e. when the second term in the denominator, $K(C_{gNO_2}/C_{gNO}) \gg 1$, Eq. (11) is simplified further

$$r = \left\{ \frac{\tilde{k}_3 K_1}{K_2} \right\} \frac{C_{gNO} C_{gO_2}}{C_{gNO_2}} = k \frac{C_{gNO} C_{gO_2}}{C_{gNO_2}} \tag{12}$$

This expression has the same apparent reaction orders for NO, O_2, and NO_2 that were determined experimentally by Mulla et al. [15]. The use of a rate expression is beneficial since no surface concentrations need to be calculated. This decreases the number of overall equations, saving computational effort during the solution process.

One important point to make about the oxidation reaction mechanism is that for this model we have only considered the forward rate of reaction. For the conditions of interest, the system is run far from equilibrium where the forward rate dominates. Also, the kinetics of the reverse reaction have not yet been well established through our experimental studies. The overall reaction, however, is reversible and a more detailed discussion of the thermodynamics and reversibility of this reaction can be found in a previous publication by Mulla et al. [15].

The results obtained for reaction expressions (11) and (12) show that both expressions are capable of quantitatively predicting the conversions obtained experimentally. Fig. 2 shows the model predicted conversion versus experimentally observed conversions using the rate expression (11). The low conversions shown in the plots are representative of the

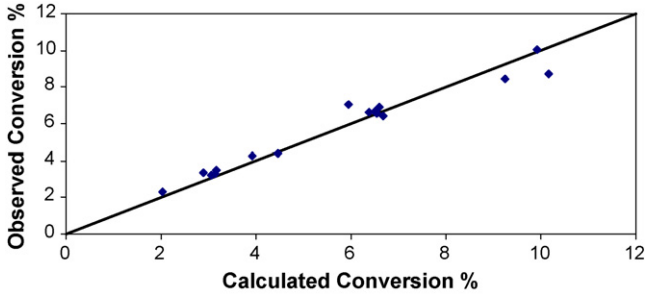

Fig. 2. Experimentally observed conversions versus predicted conversions for NO oxidation on Pt/Al_2O_3. Sixteen points were chosen from the experimental data to span the range of inlet conditions used in the experiments.

conditions run within the experimental studies. Eq. (11) is valid over a larger range of concentration values than Eq. (12), as it does not require the term in the denominator to be large compared to unity. Eq. (11) was therefore chosen for the rest of the model development.

One assumption made in the oxidation experiments was that boundary layer mass transfer was not a factor in the measurement of the rate. This is due to the high flow rates used in the experimental studies. Since the model predicts concentrations on both sides of the boundary layer, the model can be used to evaluate this assumption. Our modeling results show that largest concentration across the boundary layer occurs right at the entrance of the reactor, as expected. This is because at points further down the channel, the gas phase has had sufficient time to equilibrate with the gas in the washcoat. The model shows that the concentration difference across the boundary layer is never greater than about 3 ppm for a 300 ppm inlet NO_x concentration. Since the concentration across the boundary layer is effectively the same as the gas phase concentration (within 1%), this shows that the mass transfer does not play a significant role in the oxidation process. The process is almost entirely reaction rate controlled.

In summary, the analysis above clearly shows that the steady state rate expression for oxidation is valid and consequentially the oxidation kinetic parameters are set to the values determined previously by Mulla et al. [15]. As can be seen from the results, the NO oxidation reaction can be effectively modeled using a reaction rate expression with known parameters. Thus, there are no parameters that need to be fitted in order to describe the data. This also allows for easy coupling of the oxidation model with the storage model for describing the entire storage phase.

4.2. NO_x storage

The NO_x storage portion of the NSR process is a critical step as it allows for the engine to spend a majority of the time operating under fuel efficient lean conditions. A model on the storage process must now be developed which will give insight into phenomena that are difficult to measure. For example, mass transfer limitations and reaction kinetics are hard to study experimentally for NO_x storage, since there are transient processes. Several different mechanisms for NO_x storage were examined that include both equilibrium and non-equilibrium kinetic steps. Also, two surface models both in parallel and in series, are developed in order to account for diffusion processes within the catalyst itself.

All the uptake models assume that NO_2 is the only NO_x species involved and the experiments are performed with only NO_2 in the feed. This is justified through the work of Mahzoul et al. [26] that showed the storage capacity of NO_2 far exceeds that of NO. NO is incorporated in a coupled oxidation/storage model and is discussed later. This assumption along with a few others about the kinetics of the storage process is supported by the following results from DRIFTS studies performed in our laboratory.

4.2.1. DRIFTS studies

Fig. 3a shows the comparison of the DRIFTS spectra for the 2.13%Pt/20%BaO/Al_2O_3 monolith after 15 min of capture with various NO_x mixtures. The peaks in the region 1480–1330 cm^{-1} represent ionic barium nitrates [27–30] and the small peak at 1250 cm^{-1} represents a monodentate nitrate on alumina [31]. It is also noteworthy to point out the absence of peaks at ~1570 cm^{-1} and 1300 cm^{-1}, which represent a nitrate formed on a highly dispersed phase of barium [27]. The absence of this species allows us to assume that the adsorption of NO_x occurs only on one type of barium which exists in a bulk-like form.

By comparing the areas of the peaks in Fig. 3a, one can see that the majority of the total area of the spectral envelope is from the ionic barium nitrates for all NO_x mixtures. From this, we can assume that NO_x stored on alumina is relatively small and therefore does not need to be considered in the model. Also, the adsorption of NO gives an area of ionic nitrates which is much smaller than that of all other NO_x mixtures indicating the lower adsorption capacity for NO in the formation of ionic barium nitrates. We would also like to point out the slight increase in nitrate formation due to the addition of 12% O_2 to NO_2. We believe the increase is caused by the oxidation of NO produced via the disproportionation reaction which in turn forms more nitrates increasing their intensity observed via DRIFTS. This will be discussed further in Section 4.3.

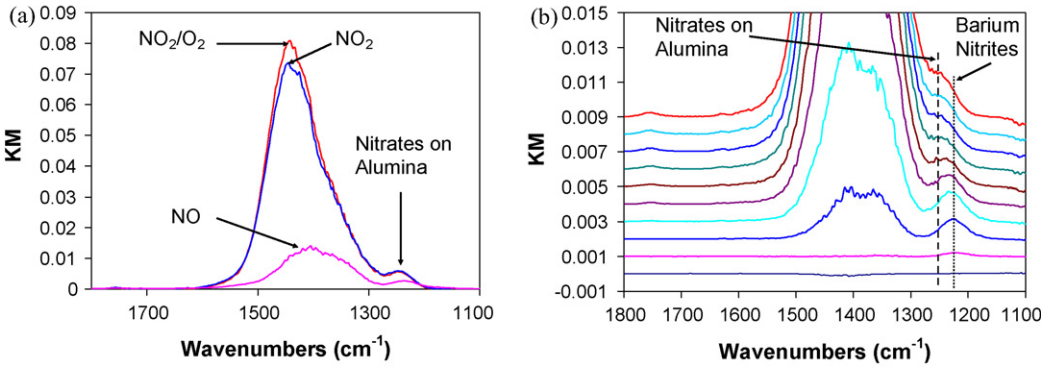

Fig. 3. (a) Reproducible DR spectra after 15 min of capture at 300 °C with 376 ppm NO or NO_2 and 12% O_2. (b) Time dependent DR spectra for the first 2 min of capture with 376 ppm NO_2/12% O_2 at 300 °C. The time between each spectrum is 12.78 s and the *y* axis is shifted for clarity.

Fig. 3b shows the time dependent DRIFTS spectra for the first 2 min of capture for the NO_2/O_2 mixture. The dotted line ($\sim$1230 cm^{-1}) represents the peak position for barium nitrites [27–29] and its presence can be seen for only the first five data points which correspond to the first minute of capture. After this point, all the barium nitrites have been oxidized to barium nitrates, indicated by the absence of this peak at later capture times. Since barium nitrites are only present during the initial stages of capture with NO_2/O_2, their formation can be neglected in the adsorption of NO_2 in the model.

4.2.2. NO_x storage modeling

A starting point for the NO_x uptake model is to assume that the adsorption is just a simple reversible adsorption reaction. Transient kinetics that allow for both adsorption and desorption are modeled as

$$NO_2 + * \underset{k_b}{\overset{k_f}{\rightleftharpoons}} NO_2* \tag{13}$$

where k_f is the adsorption rate constant and k_b is the desorption rate constant.

Fig. 4 shows typical modeled NO_x breakthrough curves for reversible adsorption along with experimental data on $Pt/BaO/Al_2O_3$. The parameters for this model were not optimized. The inlet gas consisted of 300 ppm NO_2, 10% O_2 and balance N_2. As illustrated in Fig. 4, the shape of the breakthrough curve is affected by two constants within the model, namely, the equilibrium constant, $K = k_f/k_b$, and the mass transfer coefficient, k_m. Furthermore, k_m is not an adjustable parameter, since it is determined through the use of a correlation, however, it can be varied in the model to examine the effect of mass transfer. The effect of increasing K on the breakthrough curve is to shift the curve to the right without changing the shape significantly. The effect of increasing the mass transfer rate is to increase the slope of the rise in the curve and to slightly increase the initial breakthrough time. This gives insight into the possibility that boundary layer mass transfer could be important in describing the NO_x uptake phenomena.

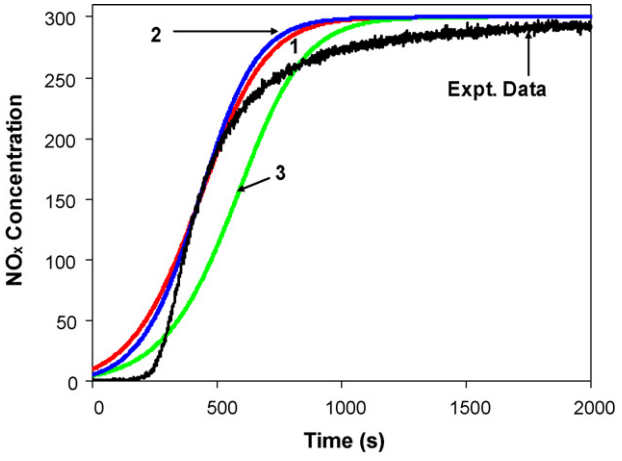

Fig. 4. NO_x breakthrough curves for the reversible adsorption model. Inlet consists of 300 ppm NO_2, 10% O_2 and balance inert. Curve 1 shows typical model result ($k_f/k_b = 125$, $k_m = 0.25$), curve 2 shows effect of increasing the mass transfer coefficient ($k_f/k_b = 125$, $k_m = 0.5$) and curve 3 shows the effect of increasing the equilibrium constant ($k_f/k_b = 167$, $k_m = 0.25$).

As can be seen, the reversible model predicts a symmetric breakthrough curve; i.e. the curvature at the beginning of breakthrough is similar to that curvature at the top of the curve approaching saturation. The reversible model is not capable of producing the asymmetry of the experiment, which shows a substantially slower approach to saturation compared to the initial rise at the bottom of the breakthrough curve.

The shape of the experimental curves suggests that another phenomenon with an additional time constant controls the process during the later portion of the breakthrough. Both the equilibrium and reversible adsorption models can be extended further by including the effects of mass transfer within the catalyst washcoat. Several groups have reported the importance of this phenomenon to the NO_x storage process and have included it in their models [4,7]. These models use a shrinking core type approximation in which the adsorption rate is dependent upon the coverage in the BaO particles. Here we propose a much simpler scheme to account for these diffusion processes, namely, a two surface (or two layer) approximation. The first surface or layer is assumed to contain the sites onto which NO_2 adsorbs first. The rate of adsorption on this surface is controlled by a typical reversible reaction as in the previous model. Once the NO_2 is adsorbed on the first layer, it can diffuse to the second layer; a process described by a mass transfer coefficient, k_{m2}. This coefficient is much smaller than a typical gas phase coefficient as it represents diffusion within the solid BaO particles. The two surfaces represent the two time constants of the NO_x uptake process. There is fast initial adsorption followed by slower diffusion to the second layer that is controlled by the second mass transfer coefficient. The equation describing the uptake to the second surface is as follows:

$$\frac{\partial C_{i2}}{\partial t} = k_{m2}(C_{i1} - C_{i2}) \tag{14}$$

where C_{i1} and C_{i2} are the concentrations on surface 1 and layer 2, respectively and k_{m2} is the second mass transfer coefficient.

Some groups have also postulated that the Ba sites near the Pt particles are more active in storing NO_2 than the Ba sites that are further away [3,26]. The NO_2 can diffuse on the surface from the Pt to nearby Ba particles. However, the NO_2 must desorb, migrate and re-adsorb to get to the Ba particles that are not within the vicinity of Pt. This Pt/Ba vicinity effect would intuitively lead to the development of a model that has both fast and slow adsorption sites on the storage component. We have developed a parallel two site model to account for this postulated structure of the catalyst. This parallel model is similar to the reversible adsorption model, but where there is another set of sites for NO_x adsorption on the surface. However, for the parallel model, both the fast and slow adsorptions are assumed to be irreversible based on some of our experimental studies and to minimize the number of parameters. The following reactions summarize the adsorption steps in the

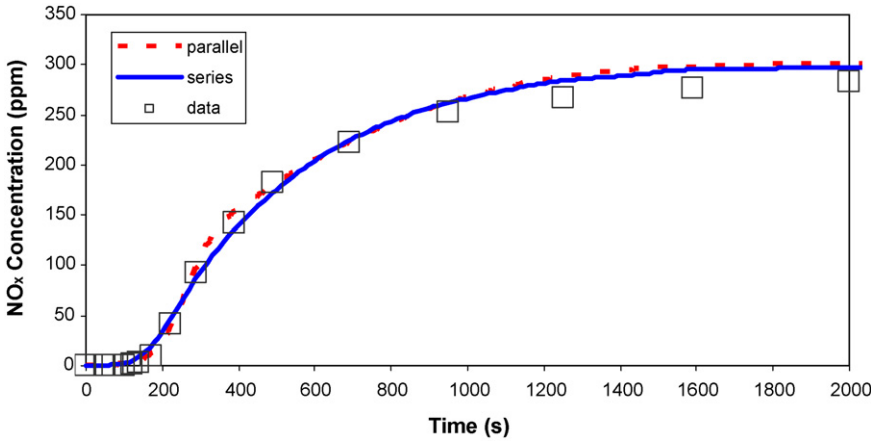

Fig. 5. Experimental NO_x breakthrough curve and model fit for series and parallel model using least squares fitting procedure (Table 2). Inlet conditions: 300 ppm NO_2, 10% O_2 and balance inert.

parallel model

$$NO_2 + S_1 \xrightarrow{k_1} (NO_2)S_1 \quad (15)$$

$$NO_2 + S_2 \xrightarrow{k_2} (NO_2)S_2 \quad (16)$$

where S_1 represents the fast adsorption sites near Pt, and S_2 represents the slow adsorption sites far away from the Pt particles.

Since our objective here is to show that the parallel model can reproduce the asymmetric nature of the NO_x breakthrough curves, we have assumed for simplicity that the adsorption steps, (15) and (16), are irreversible. Under substantial NO_2 concentrations these reactions can be driven far to the right. There will be some points at which the reversibility will come into play (low NO_2 concentration); however, the irreversible assumption is sufficient to illustrate the parallel approach. In the final series and coupled (oxidation and storage) models, these steps are taken to be reversible.

To test the parallel and series models, uptake experiments were run at 573 K and at multiple NO_2 inlet concentrations. The O_2 concentration was fixed at 10%. Optimized fits of the model parameters were obtained for the inlet NO_2 concentration at 300 ppm. We chose to fit the parameters only at these inlet conditions because these are the typical steady state conditions found in an actual engine. Having the fit at only these conditions ensures the model is the most accurate in this region. This then allows for the model to be tested at other conditions by making predictions and comparing with the data. These predictions are discussed below. Fig. 5 summarizes these results for the parallel and series models, both of which are capable of predicting the experimentally observed breakthrough profiles. The assumption of a second time constant controlling the later half of the breakthrough seems to be correct. However, we cannot yet distinguish whether this phenomenon is occurring because of bulk diffusion (i.e. the series model) or because of multiple adsorption sites (i.e. the parallel model).

One important point to consider is whether or not boundary layer mass transfer plays a role in the shape of the breakthrough curves. As discussed above, the model predicts the concentrations on both sides of the boundary layer, and can be used to determine the extent of this effect. Fig. 6 is a plot of the concentration difference across the boundary layer for the same conditions as in Fig. 5. Unlike NO oxidation, NO_x storage is greatly affected by the mass transfer through the boundary layer. The greatest effect occurs at early times and at short distances down the channel as expected. The concentration difference is as high as 60 ppm, which is a significant fraction of the inlet NO_2 concentration (311 ppm). The surface begins to saturate further down the channel, the concentration becomes less pronounced, but is still appreciable. The effect of mass transfer limitations through the boundary layer is important when considering the actual use of the NSR catalyst, since the cycle times are in the region in which the mass transfer effect is the greatest. These results suggest that a simple kinetic model alone is not enough to describe the behavior of the storage component of the NSR system at these conditions since part of the process is controlled by mass transfer.

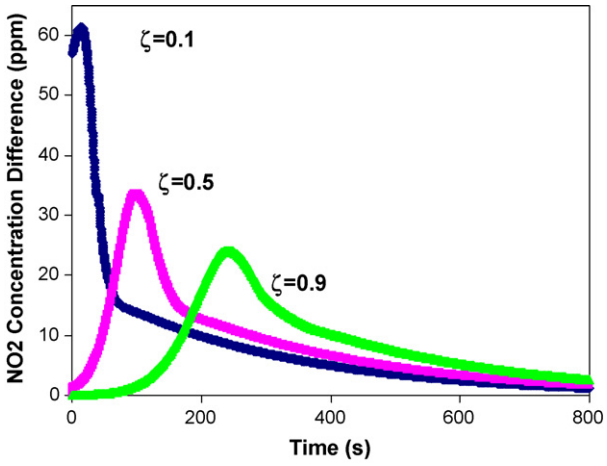

Fig. 6. NO_2 concentration difference across the boundary layer for the series model. Shows effect of boundary layer mass transfer on NO_x uptake. Inlet conditions: 311 ppm NO_2, 10% O_2, and the balance inert. ζ represents dimensionless distance down the channel.

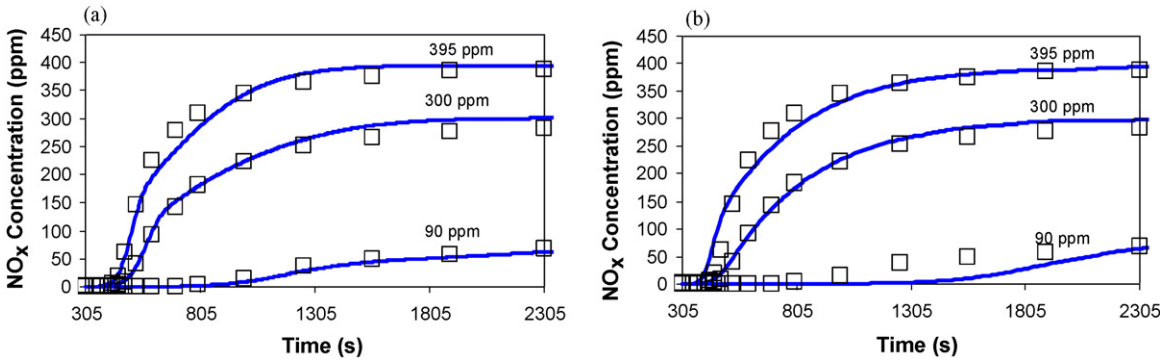

Fig. 7. (a) NO_x uptake curves for the parallel model at multiple inlet concentrations. Model parameters were fit to the data at 300 ppm and held fixed for the other two curves. (b) NO_x uptake curves for the series model at multiple inlet concentrations. Model parameters were fit to the data at 300 ppm and held fixed for the other two curves.

Once the model was fit to the data at 300 ppm, the parameters were held fixed, and the model was used to simulate the response to different inlet concentrations to test the model's ability to make valid predictions under changing experimental conditions. The parallel and series models are compared to experiments run at NO_2 inlet concentrations of 395 ppm and 90 ppm in Fig. 7a and b. As can be seen from the data, both models do a fairly good job of making predictions for inlet concentrations that are outside of the range where the parameters were fit. However, it appears that the series model does a slightly better job at high concentrations, while the parallel model does a slightly better job at lower concentrations. Although both the series and parallel models describe the uptake data, there are limitations to the models. First, neither model considers the formation of nitrites and conversion of nitrites to nitrates [2]. Also, no surface diffusion or NO_2 desorption from the platinum is considered.

Several different routes have been discussed in the literature on modeling the storage part of the NSR process [4,7,11,13,32]. These include having either reversible or equilibrium adsorption, and accounting for diffusion into the bulk. The approach reported in this paper was to construct the simplest model consistent with the data, using a ''building up'' technique. This approach started with the simplest possible model and added complexity only as needed until the model was capable of making satisfactory predictions.

The inclusion of a second adsorption time constant is perhaps the most important addition to the uptake models. Whether this is described by diffusion into the bulk, or by Pt/Ba (or K) proximity considerations, the experimental results show that this effect cannot be ignored. Modeling attempts of both equilibrium and reversible adsorption failed to match the experimental results when the second time constant was not considered. We addressed this phenomenon by developing a simple model of both the proximity of neighboring catalytic sites and bulk diffusion. These issues are addressed extensively in the literature [2,28,33–36], and it is most likely that both phenomena occur in the real system.

The advantage that our model brings is the simplicity with which it is implemented. The goal is to have a model that can eventually be solved faster than real time. This allows the model to be used within an engine control loop. Since our goal is to avoid unnecessary complications that would slow the computation, it is important to only add chemistry to the model as necessary, but in ways that are still physically reasonable. The addition of a second layer, or second adsorption site, is chemically relevant. As can be seen from the results, the addition of the second layer can be just as effective as a more complex description of the diffusion into the washcoat since its predictions of the data are quantitatively accurate.

4.3. Coupled oxidation and storage

In order to get a more complete description of the actual NO_x storage process, a coupled model including both NO oxidation and NO_x storage has also been developed. This coupling is straightforward since the oxidation model requires no parameter fitting and therefore can easily be added to the storage model. For the coupled model, we used the two sites in series model for the storage component. A NO generation term has been added, in which NO evolution is seen for every three NO_2 molecules associated with storage. In the literature, this has been attributed to a proposed disproportionation reaction [33,37,38]; specifically,

$$BaO + 3NO_2 \rightarrow Ba(NO_3)_2 + NO \quad (17)$$

This stoichiometry has been added to the NO_2 adsorption step while still keeping the adsorption reaction rate 1st order in NO_2 concentration. In other words, the rate of NO production is simply equal to 1/3 the rate of NO_2 adsorption. One additional adsorption step has been added to account for the adsorption of NO, which adsorbs in much smaller amounts than NO_2 [2]. This step was added during early development of the model in order to produce the proper NO breakthrough curves seen experimentally. Also, we have experimentally observed a significant amount of NO storage in the absence of O_2 in the feed, indicating that the catalyst has some capacity for both NO and NO_2. Our experimental studies also show that H_2O and CO_2 have a significant impact on NO_x storage which are not considered in this current work, since this initial study focused on NO_x storage without all the complications encountered with a real exhaust gas.

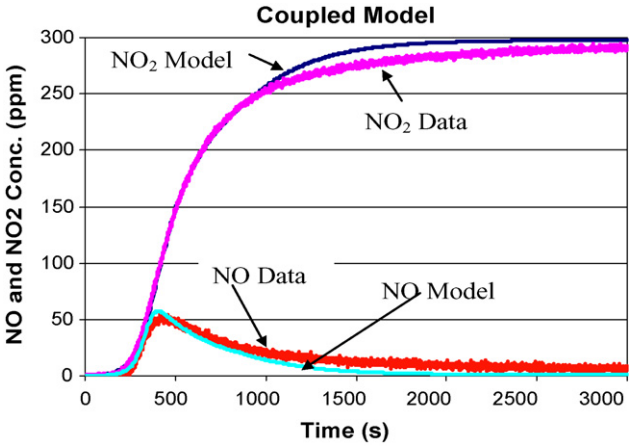

Fig. 8. Calculated and experimental NO_x breakthrough curves for the coupled model. Inlet conditions: 298 ppm NO_2, 10% O_2 and balance inert.

Fig. 8 shows typical results for the coupled model. The model output is also compared with experimental data for concentrations of NO and NO_2. The model does a good job of predicting the height of the peak that is seen for the outlet of NO. It seems that the 3 to 1 stoichiometry used for the release of NO quantitatively captures the data. The model also accurately determines the time until first breakthrough and the initial rise of the outlet concentrations. These early times are the most important for industrial use of the NSR catalyst, as the cycles rarely have a storage phase longer than a few minutes. The fit is still not perfect at longer times, over-predicting the outlet NO_2 concentration by about 10 ppm (i.e. about 4%). This small discrepancy is most likely due to some missing steady state chemistry such as NO_2 decomposition. However, even with the missing chemistry, the coupled model is still very useful, fitting the data well in the regions that are most important in practice. These results also indicate that the two layer assumption employed for the lumped storage models is still adequate.

In summary, the coupled model is an attempt at describing all of the major phenomena that occur during the uptake stage of the NSR system. Putting both steps together was straight forward, since the phenomena are decoupled and independently characterized. This again illustrates the "building up" approach to model development. The major addition to the coupled model was the inclusion of a storage step for NO. Without this step, the maximum seen in the NO concentration could not be predicted. Some researchers choose to neglect NO completely on the assumption that all of the NO gets oxidized to NO_2 at a fast enough rate to be neglected [13]. This assumption can be rationalized perhaps in the presence of water, where it is thought that the NO adsorption sites in alumina get blocked by adsorption of the water. However, by examining the experimental data in situations without H_2O, one can see that NO adsorption must be accounted for and cannot be assumed to be negligible. Even when the feed consists of only NO_2 there is still a significant output of NO at the end of the monolith. Also, some of our preliminary experimental evidence suggests that NO does get stored on the catalyst surface, albeit in smaller amounts compared to NO_2. This adsorption is probably in the form of nitrites which have been seen in a number of experimental studies [25,29].

5. Conclusion

Mathematical models of NO oxidation, NO_x storage and the coupled phenomena of NO oxidation and NO_x storage have been developed assuming, for this initial model, the absence of CO_2 and H_2O. Experimental studies of both oxidation and storage in monolith catalysts were used as a guide in the model development. The kinetics incorporated into the model have been chosen to maintain simplicity, while still including the important aspects of the chemistry as indicated by experimental studies.

Modeling of various mechanisms and steady state reaction expressions for NO oxidation has been used to develop the NO oxidation model. It has been shown through the use of detailed experimental kinetic analysis that the rate of oxidation may be described accurately through the use of a steady state rate expression as long as the process under real conditions is not mass transfer controlled. The model has shown this to be the case and thus a simple rate expression was incorporated into the final model for NO oxidation.

Modeling of NO_x storage suggested that the process is controlled by multiple time constants, yielding the asymmetric NO_x breakthrough curves seen experimentally. Two storage models were developed that capture this effect quite well, namely, a two sites in series model and a two sites in parallel model. The series model was developed to represent diffusion into the bulk of the capture phase, while the parallel model was developed to represent slow and fast adsorption sites on the surface. It has also been shown that boundary layer mass transport plays a significant role in the shape of the breakthrough curves. Any model of an NSR monolith catalyst, for the range of conditions studied here, must include mass transfer limitations across the boundary layer.

Acknowledgements

The authors would like to thank Cummins, Inc. as well as the Indiana 21st Century Research and Technology Fund for Financial support of this work.

References

[1] W. Bogner, M. kramer, B. Krutzsch, S. Pischinger, D. Voigtlander, G. Wenninger, F. Wirbeleit, M.S. Brogan, R.J. Brisley, D.E. Webster, Appl. Catal. B 7 (1995) 153–171.
[2] W.S. Epling, L.E. Campbell, A. Yezerets, N.W. Currier, J.E. Parks, Catal. Rev. 46 (2004) 163.
[3] N. Takahashi, H. Shinjoh, T. Iijima, T. Suzuki, K. Yamazaki, K. Yokota, H. Suzuki, N. Miyoshi, S.-I. Matsumoto, et al. Catal. Today 27 (1996) 63–69.
[4] L. Olsson, R.J. Blint, E. Fridell, Ind. Eng. Chem. Res. 44 (2005) 3021–3032.
[5] L. Olsson, E. Fridell, M. Skoglundh, B. Andersson, Catal. Today 73 (2002) 263–270.
[6] L. Olsson, H. Persson, E. Fridell, M. Skoglundh, B. Andersson, J. Phys. Chem. B 105 (2001) 6895–6906.

[7] U. Tuttlies, V. Schmeisser, G. Eigenberger, Top. Catal. 30–31 (2004) 187–192.
[8] P. Koci, M. Schejbal, J. Trdlicka, T. Gregor, M. Kubicek, M. Marek, Catal. Today 119 (2006) 64–72.
[9] P. Koci, M. Marek, M. Kubicek, T. Maunula, M. Harkonen, Chem. Eng. J. 97 (2004) 131–139.
[10] M. Crocoll, S. Kureti, W. Weisweiler, J. Catal. 229 (2005) 480–489.
[11] C.S. Daw, K. Chakravarthy, K.E. Lenox, in: Proceedings of the Third Joint Meeting of the U.S. Sections of The Combustion Institute, 2002.
[12] C.J.P. Laurent, F.H. Mahzoul, L. Delfosse, P. Gilot, Chem. Eng. Sci. 58 (2003) 1793.
[13] M. Sharma, M.P. Harold, V. Balakotaiah, Ind. Eng. Chem. Res. 44 (2005) 6264–6277.
[14] S.S. Mulla, N. Chen, L. Cumaranatunge, W.N. Delgass, W.S. Epling, F.H. Ribeiro, Catal. Today (2005) accepted.
[15] S.S. Mulla, N. Chen, W.N. Delgass, W.S. Epling, F.H. Ribeiro, Catal. Lett. 100 (2005) 267–270.
[16] T.J. Toops, D.B. Smith, W.S. Epling, J.E. Parks, W.P. Partridge, Appl. Catal. B 58 (2005) 255–264.
[17] A.A. Phatak, N. Koryabkina, S. Rai, J.L. Ratts, W. Ruettinger, R.J. Farrauto, G.E. Blau, W.N. Delgass, F.H. Ribeiro, Catal. Today 123 (2007) 224–234.
[18] R.L. Muncrief, P. Khanna, K.S. Kabin, M.P. Harold, Catal. Today 98 (2004) 393–402.
[19] P. Stone, M. Ishii, M. Bowker, Surf. Sci. 537 (2003) 179–190.
[20] H. Tsukahara, T. Ishida, M. Mayumi, Nitric Oxide 3 (1999) 1198–1991.
[21] R.E. Hayes, S.T. Kolaczkowski, Catal. Today 47 (1999) 295–303.
[22] FEMLAB 3 Multiphysics Modeling, 3.1.0.157 ed., COMSOL Inc., Burlington, MA, 1994–2004.
[23] MATLAB, 7.0.1.24704 ed., MathWorks Inc., Natick, MA, 1984–2004.
[24] R. Burch, T.C. Watling, J. Catal. 169 (1997) 45–54.
[25] E. Fridell, H. Persson, L. Olsson, B. Westerberg, A. Amberntsson, M. Skoglundh, Top. Catal. 16–17 (2001) 133–137.
[26] H. Mahzoul, J.F. Brilhac, P. Gilot, Appl. Catal. B 20 (1999) 47–55.
[27] J. Szanyi, J.H. Kwak, J. Hanson, C. Wang, T. Szailer, C.H.F. Peden, J. Phys. Chem. B 109 (2005) 7339–7344.
[28] I. Nova, L. Castoldi, L. Lietti, E. Tronconi, P. Forzatti, F. Prinetto, G. Ghiotti, J. Catal. 222 (2004) 377–388.
[29] C. Sedlmair, K. Seshan, A. Jentys, J.A. Lercher, J. Catal. 214 (2003) 308–316.
[30] P.T. Fanson, M. Horton, R.W.N. Delgass, J. Lauterbach, Appl. Catal. B: Environ. 46 (2003) 393–413.
[31] T.J. Toops, D.B. Smith, W.P. Partridge, Appl. Catal. B: Environ. 58 (2005) 245–254.
[32] F. Laurent, C.J. Pope, H. Mahzoul, L. Delfosse, P. Gilot, Chem. Eng. Sci. 58 (2003) 1793–1803.
[33] N.W. Cant, M.J. Patterson, Catal. Today 73 (2002) 271–278.
[34] X. Li, M. Meng, P. Lin, Y. Fu, T. Hu, Y. Xie, J. Zhang, Top. Catal. 22 (2003) 111–115.
[35] X. Chen, J. Schwank, J. Li, W.F. Schneider, J. Goralski, T. Christian, P.J. Schmitz, Appl. Catal. B 61 (2005) 164–175.
[36] W.S. Epling, J.E. Parks, G.C. Campbell, A. Yezerets, N.W. Currier, L.E. Campbell, Catal. Today 96 (2004) 21–30.
[37] S. Hodjati, C. Petit, V. Pitchon, A. Kiennemann, Appl. Catal. B 27 (2000) 117–126.
[38] J. Despres, M. Koebel, O. Krocher, M. Elsener, A. Wokaun, Appl. Catal. B 43 (2003) 389–395.